Cancer Research

Oncogenic Mutation of AIMP2/p38 Inhibits Its Tumor-Suppressive Interaction with Smurf2

Dae Gyu Kim[1], Jin Young Lee[1], Ji-Hyun Lee[1], Ha Yeon Cho[2], Beom Sik Kang[2], Song-Yee Jang[3], Myung Hee Kim[3], Min Guo[4], Jung Min Han[5], Seong-Jin Kim[6], and Sunghoon Kim[1,7]

Abstract

AIMP2/p38 is a multifunctional tumor suppressor that normally resides in the cytosol as a scaffold protein of the multi-tRNA synthetase complex (MSC). One of the tumor-suppressive functions of AIMP2 is to facilitate ubiquitin-mediated degradation of FUSE-binding protein (FBP, FUBP1), a transcriptional activator of c-Myc. However, the mechanism by which AIMP2 functions within this pathway and its significance in tumorigenesis are uncertain. Here, we report that Smurf2 is responsible for AIMP2-mediated ubiquitination of FBP, and a mutation in AIMP2 that inhibited its nuclear interaction with Smurf2 enhanced cellular transformation and tumorigenesis *in vivo*. Treatment of HeLa cells with TGFβ resulted in the phosphorylation of AIMP2 on S156, a residue that is exposed on the embedded GST domain of AIMP2. We further found that phospho-AIMP2 dissociated from the MSC and translocated to the nucleus, where it bound to Smurf2, enhancing ubiquitination of FBP. AIMP2 also inhibited nuclear export of Smurf2 to sustain TGFβ signaling. Collectively, these findings present a novel tumor-suppressive interaction between AIMP2 and Smurf2 and suggest that the disruption of this interaction can lead to oncogenic transformation. *Cancer Res; 76(11); 3422–36. ©2016 AACR.*

Introduction

TGFβ signal is involved in the regulation of diverse cellular functions, including cell proliferation, differentiation, migration, and apoptosis (1, 2). Alteration of TGFβ signaling can lead to human diseases, such as fibrosis and cancer (3–5). TGFβ signaling is initiated by the activation of TGFβ receptor II. Activated type II receptor recruits and phosphorylates TGFβ receptor I (TβRI), which propagates the signal via phosphorylation of Smad proteins. Then, phosphorylated Smad2 and Smad3 (R-Smad) form the complex with Smad4 (Co-Smad) and translocate into the nucleus to regulate gene transcription (6). Duration and stability of TGFβ signaling is tightly regulated via negative feedback loop. Negative feedback loop of TGFβ signaling is composed of Smad7 (I-Smad; ref. 7) and Smad ubiquitin regulatory factors 2 (Smurf2), HECT type E3 ubiquitin ligase (8, 9). To terminate the signal, Smurf2 is activated by the interaction of Smad7 in nucleus. The Smad7–Smurf2 complex is subsequently exported from nucleus and targeted to TβRI in plasma membrane (10). Smurf2 then delivers ubiquitin to TβRI for proteasomal degradation (11). The reduction of TβRI leads to the termination of TGFβ signaling and inhibits the excess proceeding of signal. For this reason, Smurf2 is known as a negative regulator of TGFβ signal pathway. However, it was recently shown to exert tumor-suppressive function by controlling genome stability via the ubiquitin-dependent turnover of RNF20 (12). Although this result suggests that Smurf2 may have additional functions in nucleus, it is not understood yet how its activity is determined in the context of TGFβ signal.

Aminoacyl-tRNA synthetases (ARS) are the enzymes that ligate the amino acids to their cognate tRNAs. In eukaryotes, nine different ARSs form a macromolecular complex with three auxiliary factors, AIMP1/p43, AIMP2/p38, and AIMP3/p18 (13) that play a scaffolding role of the whole complex (14). Among AIMPs, AIMP2 induces cell death by the activation of p53 (15) and by downregulation of TRAF2 (16) in response to DNA damage and TNFα signal, respectively. Reduced expression of AIMP2 showed enhanced susceptibility to tumor formation in mouse carcinogenesis models, suggesting AIMP2 as a haploinsufficient tumor suppressor (17). Upon TGFβ stimulation, AIMP2 reduces the cellular level of FBP (far upstream element–binding protein), a transcriptional activator of c-Myc (18), resulting in the downregulation of c-Myc transcription (19). However, little is known on how its nuclear translocation is triggered and how ubiquitination of FBP is achieved. In this work, we found the unexpected functional connection of Smurf2 with AIMP2 and suggest their molecular interaction based on the structural information. Cell and *in vivo* analyses also demonstrated the functional significance of the Smurf2–AIMP2 interaction for the control of tumorigenesis.

[1]Medicinal Bioconvergence Research Center, College of Pharmacy, Seoul National University, Seoul, Korea. [2]School of Life Science and Biotechnology, Kyungpook National University, Daegu, Korea. [3]Infection and Immunity Research Center, Korea Research Institute of Bioscience and Biotechnology, Daejeon, Korea. [4]Department of Cancer Biology, Scripps Research Institute, Florida Campus, Jupiter, Florida. [5]College of Pharmacy, Yonsei University, Seoul, South Korea. [6]CHA Research Institutes & CHA Cancer Institute, CHA University, Seongnam, Korea. [7]Department of Molecular Medicine and Biopharmaceutical Sciences, Graduate School of Convergence Science and Technology, Seoul National University, Seoul, Korea.

Note: Supplementary data for this article are available at Cancer Research Online (http://cancerres.aacrjournals.org/).

Corresponding Author: Sunghoon Kim, Seoul National University, Kwanak-ro 599, Kwanak-gu, Seoul 151-742, Korea (South). Phone: 822-880-8180; Fax: 822-875-2621; E-mail: sungkim@snu.ac.kr

doi: 10.1158/0008-5472.CAN-15-3255

Materials and Methods

Cell culture and materials

Human embryonic lung fibroblast cell line, WI-26, was obtained from Korea Cell Line Bank, and other cell lines were purchased from the ATCC. AIMP2 knockout (KO) mouse embryonic fibroblasts (MEF) were isolated from 12.5- to 14.5-day embryos. Cell lines (WI-26, 293T, HeLa, and MEFs) were cultured in DMEM or other cell lines in RPMI1640 media complemented with 10% FBS and 1% penicillin/streptomycin in 5% CO_2 at 37°C. Human Myc-AIMP2 was cloned at the EcoRI/XhoI sites of pcDNA3.0. FLAG-TβRI and GFP-Smad7 were kind gifts from Dr. Seong Jin Kim (CHA University, Korea). 3xFLAG-Smurf1 and FLAG-Smurf2 wild-type (WT), deletion mutants were kindly provided by Dr. Suk-Chul Bae (Chungbuk National University, Cheongju, South Korea). Myc-, GFP-, Strep-, His- and GST-AIMP2–containing point mutations were cloned using QuikChangeII (Agilent), following the manufacturer's instruction. The siRNA-targeting AIMP2 was designed with the sequence of AGAGCUUGCAGAGACAGGUUAGACU. The cells were separated to cytosolic and nuclear fractions using ProteoExtract Kit (Calbiochem), following the manufacturer's instruction. TGFβ1 (5 ng/mL) was purchased from R&D Systems. MG132 was purchased from Calbiochem; SB202190, SP600125, leptomycin B (LMB), and anti-FLAG antibody from Sigma-Aldrich; anti-AIMP2 antibody from Abcam; and anti-p-Smad2 and -Smad2 antibodies from Cell Signaling Technology. The other antibodies and siRNAs against Smurf2 and CRM1 were purchased from Santa Cruz Biotechnology.

Coimmunoprecipitation

The cells were lysed with 50 mmol/L Tris-HCl (pH 7.4) buffer containing 100 mmol/L NaCl, 0.5% Triton X-100, 0.05% SDS, 10% glycerol, 1mmol/L EDTA, and protease inhibitor (Calbiochem). To remove the nonspecific IgG-bound proteins, protein extracts were incubated with normal IgG and protein agarose for 2 hours and centrifuged. The supernatants were mixed with specific antibody, incubated for 4 hours at 4°C with gentle agitation, and protein agarose beads were added. After agitation for 4 hours at 4°C, precipitates were washed with the cold lysis buffer three times, and precipitates were dissolved in the SDS sample buffer and subjected to SDS-PAGE.

In vitro binding assay

To detect the direct interaction, GST-tagged proteins were mixed with proteins prepared by *in vitro* translation (Promega) in the presence of [^{35}S]methionine (PerkinElmer) or cell extracts in 50 mmol/L Tris-HCl (pH 7.4) buffer containing 100 mmol/L NaCl, 0.5% Triton X-100, 10% glycerol, 1 mmol/L EDTA, and protease inhibitor (Calbiochem) for 6 hours at 4°C. After incubation, mixed GST proteins were precipitated with glutathione–sepharose beads and washed with cold upper buffer three times. Coprecipitates with GST proteins were subjected to SDS-PAGE. The separated precipitates were detected by autoradiography using BAS (FLA-3000, Fujifilm) and analyzed by MultiGauge program (V3.0, Fujifilm) or Western blotting with specific antibody.

Flow cytometry analysis

To determine the effect of AIMP2 on TGFβ-mediated cell cycle, AIMP2$^{+/+}$ (WT), AIMP2$^{-/-}$ (KO), MEFs and HeLa cells transfected with siRNA against AIMP2 were incubated in the medium containing TGFβ1 and 0.5% serum for 12 hours. After incubation, the harvested cells were fixed with 70% ethanol for 1 hour at 4°C and washed twice with cold PBS. The cells were stained with propidium iodide (50 μg/mL), 0.1% sodium citrate, 0.3% NP40, and RNaseA (50 μg/mL) for 40 minutes and subjected to flow cytometry (FACSCalibur, Becton Dickinson). For each sample, 20,000 cells were analyzed using CellQuest Pro Software.

Pulse-chase assay

The FLAG-TβRI–expressing cells were incubated with methionine-free medium for 1 hour. Then, [^{35}S]methionine (50 μCi/mL) was added and incubated for 1 hour. After washing off the radioactive methionine with fresh medium, the cells were cultivated in complete medium for 4 hours and harvested at the indicated time interval. TβRI was immunoprecipitated with FLAG antibody, and precipitates were subjected to SDS-PAGE. Autoradiography detected by using BAS (FLA-3000, Fujifilm) was quantified by MultiGauge program (V3.0, Fujifilm) and displayed as bar graph.

Ubiquitination assay

The cells were preincubated with MG132 (50 μmol/L) for 4 hours and treated with TGFβ1. The cells were lysed with 50 mmol/L Tris-HCl (pH 7.4) buffer containing 100 mmol/L NaCl, 0.5% Triton X-100, 0.1% SDS, 10% glycerol, 1 mmol/L EDTA, and protease inhibitor (Calbiochem). The target proteins were immunoprecipitated with their specific antibodies and subjected to SDS-PAGE to determine ubiquitination.

In vitro kinase assay

Active p38MAPK was prepared by immunoprecipitation using anti-p38MAPK antibody from the cells cultured in medium containing TGFβ1. The purified GST-AIMP2, His-tagged 34S AIMP2 (N-terminus 34 amino acids deletion form), and multi-tRNA synthetase complex (MSC)–containing Strep-AIMP2 was used as a substrate for kinase assay. Each substrate protein was preincubated for 30 minutes at 4°C with the active p38MAPK in buffer containing 50 mmol/L Tris-HC1 (pH 7.3), 100 mmol/L NaCl, 10 mmol/L $MnCl_2$, 10% (v/v) glycerol, 5 mmol/L dithiothreitol, and 0.05% Triton X-100. After preincubation, the reaction was carried out in the presence of [γ-^{32}P]ATP 10 μCi (3,000 Ci/mmol) at 28°C for 20 minutes and stopped by the addition of the SDS sample buffer. The proteins in the reaction mixture were separated by SDS-PAGE and autoradiographed (FLA-3000, Fujifilm).

Purification of the MSC

The gene encoding AIMP2/p38, the scaffold for the MSC was cloned into the pEXPR-IBA5 mammalian expression vector (IBA), generating a construct with an N-terminal Strep-tag II. Suspension grown Expi293 cells in 30 mL of Expi293 Expression Medium (Life Technologies) were transfected with 30 μg of the N-terminal Strep-tagged AIMP2 expression plasmid when the cell density reached 3×10^6 cells/mL. The culture medium was freshly changed with 200 to 800 μg/mL of G418 gradually every three days, until the cells expressed AIMP2 stably. The stable AIMP2-expressing Expi293F cells, which were grown in 200 mL of Expi293 Expression Medium in a 37°C incubator with humidified atmosphere of 8% CO_2 in air on an orbital shaker platform rotating at 125 rpm until the cell density reached 5×10^6 cells/mL, were centrifuged at 800 rpm at 4°C for 10 minutes. The cell pellet was then lysed in a buffer

containing 50 mmol/L Tris-HCl (pH 7.4), 7.5% glycerol, 150 mmol/L NaCl, 1 mmol/L EDTA, 0.1% NP40, 1.0% sodium deoxycholate, 0.25 mmol/L sodium pyrophosphate, 2.0 mmol/L sodium vanadate, 2.0 mmol/L sodium fluoride, aprotinin (10 μg/mL), leupeptin (10 μg/mL), pepstatin (10 μg/mL), and 0.2 mmol/L PMSF. After centrifuging at 16,000 rpm for 1 hour, the cleared lysate was applied to a 1-mL Strep-Tactin Sepharose Column (IBA). The resin was washed thoroughly with the washing buffer, which contains 100 mmol/L Tris-HCl (pH 8.0), 150 mmol/L NaCl, and 1 mmol/L EDTA. The AIMP2-interacting MSC proteins were eluted with a buffer containing 100 mmol/L Tris-HCl (pH 8.0), 150 mmol/L NaCl, 1 mmol/L EDTA, and 2.5 mmol/L desthiobiotin. The eluted MSC proteins were evaluated by SDS-PAGE.

Gel filtration chromatography

Strep-AIMP2 wild-type-, S156A-, and S156D-transfected HeLa cells were treated with TGFβ1 for 2 hours. For size-exclusion chromatography, the cells were lysed with 50 mmol/L HEPES (pH 7.6) containing 300 mmol/L NaCl, 1 mmol/L EDTA, 10% glycerol, 0.5% Triton X-100, and 1 mmol/L dithiothreitol. Cell lysates were filtered with 0.22-μm syringe filter. Proteins (1 mg) were loaded onto column (Superdex 200 10/300 GL, GE Healthcare) in AKTA FPLC system. The loaded lysates were eluted at the flow rate of 0.4 mL/minute. Proteins of each fraction were subjected to SDS-PAGE and detected by Western blotting with specific antibodies.

Thymidine incorporation

HeLa cells were introduced by transfection with Myc-AIMP2 or si-AIMP2. The transfected HeLa or AIMP2$^{+/+}$ (WT) and AIMP2$^{-/-}$ (KO) MEF cells were treated with TGFβ1 for 12 hours in the medium containing 0.5% serum. The cells were incubated with 1 μCi/mL of [^{3}H]thymidine for 4 hours. The incorporated thymidine was measured by liquid scintillation counter (Wallac), and the measured radioactivity was presented as bar graph. The experiments were repeated three times independently.

Reporter gene assay

HeLa cells expressing the luciferase gene with c-Myc promoter (Addgene plasmid 16604) and si-Smurf2 RNA were treated with TGFβ1 for 24 hours. The luciferase activity was measured by using luciferase assay system following the manufacturer's protocol (Promega). The determined activity was shown as a bar graph, and the experiments were repeated three times independently.

Immunofluorescence staining

293T and HeLa cells were expressed by using transfection with GFP-AIMP2 and RFP-Smurf2. The cells were incubated in medium containing MG-132 and TGFβ1 for 4 hours. HeLa cells were expressed with GFP-AIMP2 wild type, S156A, and S156D mutants. The cells were treated with TGFβ1 for 2 hours. After treatment, all the cells were washed briefly with cold PBS, fixed with methanol, mounted with the mounting solution containing DAPI (ImmunoBioScience Corp.), and observed by confocal laser-scanning microscopy.

Quantitative RT-PCR

The expression of AIMP2 was regulated by transfection with Myc-AIMP2 and siRNA-targeting AIMP2. After transfection, the cells were treated with TGFβ1. Total RNAs were extracted using an RNeasy Mini Kit (Qiagen) and used for RT-PCR with random hexamer, dNTP, and Moloney murine leukemia virus. Then, 1 μL of cDNA was used for qPCR (7500 Fast Real-Time PCR System) to detect the mRNA expression of TβRI. The sequence of primer specific to TβRI and GAPDH are as following; TGFβ receptor I, TGTTGGTACCCAAGGAAAGC, CACTCTGTGGTTTGGAGCAA; GAPDH, AGCCACATCGCTCAGACAC, GCCCAATACGACCAAATCC.

Real-time cell monitoring

A549 stable cells (2×10^3) were seeded in 48-well plates. When the morphology was formed, the cells were subjected to real-time monitoring system (IncuCyte, Essen BioScience). The image and number of cells were captured and measured in every 2 hours for 42 hours, respectively.

Anchorage-independent colony-forming assay

A549 stable cells were used for anchorage-independent colony-forming assay. The cells were diluted into RPMI medium containing 10% FBS and 0.3% agar. The diluted cells (200 cells) were seeded into 12-well plates (TPP) coated with 0.6% agar. The medium was changed in every 3 days. After 6 weeks, the settled colonies were stained with hematoxylin (Sigma-Aldrich), and the numbers of colonies were measured. The experiments were performed three times independently.

In vivo tumorigenesis

A549 cells stably expressing AIMP2 WT, S156A, and S156D mutants were established by the treatment of G418 for 1 month. Cellular levels of the ectopically expressed AIMP2 proteins were compared by Western blotting. The selected stable cells (2×10^6) were subcutaneously injected into the back of 7-week-old female BALB/cAnCr nude mice ($n = 10$/group). After two months, mice were sacrificed and the embedded tumors analyzed. The size and weight of isolated tumor were measured, and they were subjected to immunoblotting analysis with the indicated antibodies.

Results

Nuclear interaction of Smurf2 and AIMP2

To have an insight into the potential E3 ligase that is responsible for AIMP2-dependent ubiquitination of FBP, we searched STRING, which is the database for known and predicted protein–protein interactions, and identified several different E3 ubiquitin ligases that could be linked to AIMP2 via ubiquitin C (Fig. 1A). Among them, Smurf2 is known to play a key role in TGFβ signal and delivers ubiquitin to target proteins in nucleus (10). To confirm this possibility, we tested the TGFβ-dependent interaction of Smurf2 with AIMP2 using coimmunoprecipitation. We transfected Flag-Smurf2 and -Smurf1, Myc-PARK2, and -TRAF6 with Strep-AIMP2 into HeLa cells and incubated the transfectants in the absence and presence of TGFβ. Then, AIMP2 was immunoprecipitated with Strep-tag column, and coprecipitated proteins were determined with the antibodies against the attached tags. The results showed that among the four tested E3 ligases, Smurf2 showed TGFβ-dependent interaction with AIMP2 (Fig. 1B). In contrast, Smurf1 did not bind to AIMP2, whereas both of PARK2 and TRAF6 bound to AIMP2 independently of TGFβ treatment. We further examined the interaction of endogenous AIMP2 and Smurf2 by coimmunoprecipitation and found

the interaction of the two proteins in the nuclear fraction in the presence of TGFβ1 (Fig. 1C). The direct interaction of the two proteins was shown by *in vitro* pulldown assay, in which radioactively labeled AIMP2 was coprecipitated with GST-Smurf2 but not with GST (Fig. 1D). To see whether the cellular localization of AIMP2 and Smurf2 is affected by TGFβ signal, we introduced GFP or GFP-AIMP2 with RFP-Smurf2 into HeLa cells, incubated the cells in the absence and presence of TGFβ, and monitored the cellular distribution of the two proteins by fluorescence microscopy. Although the majority of Smurf2 was located in nucleus in the absence of TGFβ, the nuclear level of Smurf2 was significantly reduced by TGFβ treatment (Fig. 1E, left). The cellular distribution of GFP was not much changed by TGFβ treatment. In contrast, GFP-AIMP2 was mainly observed in cytosol in the absence of TGFβ; nuclear level of AIMP2 was increased and colocalized with RFP-Smurf2 by treatment of TGFβ (Fig. 1E, right). These results suggest the TGFβ-dependent interaction of AIMP2 with Smurf2 in nucleus.

To determine the peptide regions of the two proteins responsible for the interaction, we prepared various deletion and point mutants (Supplementary Fig. S1A) and tested their interactions by coimmunoprecipitation. All the deletion fragments of Smurf2 containing HECT domain showed the interaction with Myc-AIMP2 (Supplementary Fig. S1B). Then, the different fragments of AIMP2 were expressed as Myc fusion proteins and their interactions with FLAG-Smurf2 fd412 (HECT domain only) were tested by coimmunoprecipitation. The results showed that the peptide DM2 containing 84-225aa region of AIMP2 binds to Smurf2 (Supplementary Fig. S1C). We further divided the 84-225aa region of AIMP2 to four smaller fragments (Supplementary Fig. S1A; MT1-4) and tested their binding to Smurf2 by *in vitro* pulldown assay. From this analysis, we found that the 84-119aa region (MT1) of AIMP2 is mainly involved in the interaction with Smurf2 (Supplementary Fig. S1D). We also tested the interaction between Smurf2 and some of the AIMP2 mutants that were found in lung cancer cell lines (15) and found that the mutants such as PM1 (I92V) and PM2 (E97D/P98L/T99S) could not bind to Smurf2 (Supplementary Fig. S1E), further validating the significance of the peptide region (84–119) for the interaction with Smurf2 HECT domain (Fig. 1F).

Smurf2–AIMP2 complex downregulates c-Myc

We investigated the functional implication for the interaction of AIMP2 with Smurf2. As Smurf2 works as a complex with Smad7 (11), we monitored the effect of Smurf2, Smad7, and AIMP2 in different combinations on the cellular level of FBP. The FBP level was decreased by the exogenous introduction of all the three proteins, whereas it was little affected by a single or pairwise introduction of these proteins (Fig. 2A). Moreover, the FBP level was not affected when the catalytically inactive mutant of Smurf2 (CA; ref. 10) was used (Fig. 2A). Introduction of Smurf1, which does not binds to AIMP2, did not affect the AIMP2-dependent reduction of FBP (Supplementary Fig. S2A). These results suggest the specific requirement of the Smurf2 catalytic activity for the AIMP2-mediated downregulation of FBP. The TGFβ-induced interaction of Smurf2 and FBP was shown by coimmunoprecipitation of FLAG-Smurf2 and endogenous FBP (Fig. 2B). It is further confirmed by coimmunoprecipitation of the endogenous Smurf2 and FBP (Supplementary Fig. S2B). The interaction between Smurf2 and FBP was enhanced when Strep-AIMP2 was added for coimmunoprecipitation of FLAG-Smurf2 and endogenous FBP (Supplementary Fig. S2C). We also confirmed by *in vitro* pulldown assay that the interaction of Smurf2 HECT domain and FBP was increased as the increasing amount of AIMP2 was added, further validating that AIMP2 would facilitate the interaction of the two proteins (Fig. 2C). Conversely, the interaction of endogenous FBP with Smurf2 was significantly reduced in the AIMP2$^{-/-}$ (KO) MEFs and AIMP2-suppressed HeLa cells (Fig. 2D and Supplementary Fig. S2D, respectively). Deletion mapping showed that the peptide region spanning MT1 (84–119) and MT2 (120–155) of AIMP2 would be mainly involved in the interaction with FBP (Supplementary Fig. S2E).

The importance of Smurf2 for the downregulation of FBP was further tested both by Western blotting and RT-PCR. The AIMP2-dependent reduction of FBP was observed by Western blotting (Fig. 2E, top), but not by RT-PCR (Fig. 2E, bottom), suggesting that downregulation of FBP takes place at protein but not transcription level. In contrast, c-Myc level, the target gene of FBP (18), was reduced in both of Western blot and RT-PCR assays. When Smurf2 was suppressed with its specific siRNA, the effect of AIMP2 on FBP was not observed in both assays. We also checked the c-Myc transcription using luciferase reporter assay and found that the AIMP2-dependent reduction of the luciferase activity was not observed when Smurf2 expression was suppressed with its siRNA (Supplementary Fig. S2F). To see whether ubiquitin-mediated protein degradation is involved in the cellular levels of FBP, we introduced different combination of Smurf2, Smad7, and AIMP2 into HeLa cells, and the endogenous FBP was immunoprecipitated with its specific antibody and monitored ubiquitination of FBP with anti-ubiquitin antibody. The ubiquitin labeling was increased when all of the three factors were simultaneously introduced (Fig. 2F). The Smurf2/Smad7/AIMP2–induced ubiquitination of FBP was not observed when Smurf2 WT was replaced with the Smurf2 CA mutant, further confirming the requirement of the Smurf2 catalytic activity for the ubiquitination of FBP. We then examined whether the binding of AIMP2 to Smurf2 is critical for the E3 ubiquitin ligase activity of Smurf2 to FBP using various mutants of AIMP2. The AIMP2 mutants, PM1 and PM2, which could not bind to Smurf2, gave little effect on the FBP level (Supplementary Fig. S2G), indicating that the binding ability of AIMP2 to Smurf2 is critical for the downregulation of FBP.

As Smad7 is required for E3 ligase function of Smurf2 (10), we examined whether AIMP2 would affect the complex formation of Smurf2 and Smad7 using immunoprecipitation and *in vitro* pulldown assays. For immunoprecipitation assay, we introduced GFP-Smad7, FLAG-Smurf2 with and without Myc-AIMP2 into HeLa cells. We then compared the complex formation between Smurf2 and Smad7 by immunoprecipitation with anti-GFP antibody in the absence and presence of AIMP2 from TGFβ1-treated HeLa cells. The Smurf2–Smad7 complex formation was increased by the addition of Myc-AIMP2 (Supplementary Fig. S2H). For *in vitro* pulldown assay, GST-Smurf2 was mixed with [^{35}S]methionine-labeled Smad7 and the increasing amount of AIMP2, both of which were synthetized by *in vitro* translation. The GST–Smurf2 and Smad7 complex in the mixture was pulled down with glutathione-sepharose, and the effect of AIMP2 on the complex formation was monitored by autoradiography. The amount of Smad7 complexed with GFP-Smurf2 was increased according to the amount of added AIMP2

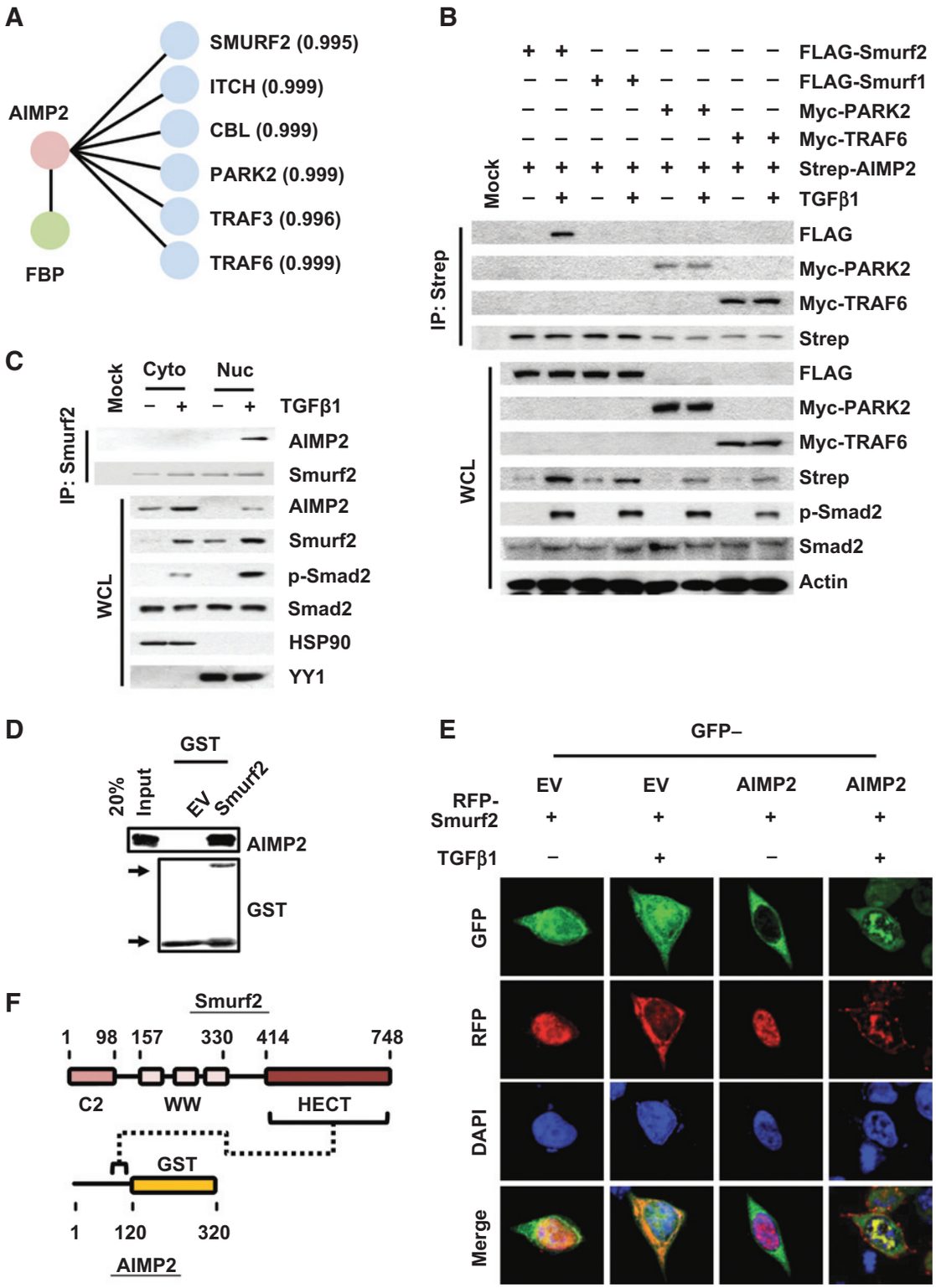

Figure 1.
TGFβ-dependent nuclear interaction of Smurf2 and AIMP2. A, mining of String database (string-db.org) for protein–protein interactions unveiled several different E3 ligases that can be associated with AIMP2 via ubiquitin C, such as SMURF2, ITCH, CBL, PARK2, TRAF3, and TRAF6. The numbers indicate the scores, suggesting the binding affinity of two proteins. B, FLAG-tagged Smurf2 and Smurf1, Myc-tagged PARK2, and TRAF6 were expressed in HeLa cells expressing Strep-AIMP2. (*Continued on the following page.*)

(Supplementary Fig. S2I). These results suggest that AIMP2 would facilitate the complex formation between Smurf2 and Smad7.

AIMP2 suppresses nuclear export of Smurf2

It is known that the Smurf2–Smad7 complex is exported from nucleus to target TβRI for degradation as negative feedback of TGFβ signaling (11). We thus examined whether CRM1 (chromosomal region maintenance 1) would affect the nuclear export of Smurf2 using LMB, an inhibitor of CRM1 that is a putative receptor of nuclear export for Smurf2 (20). The nuclear level of Smurf2 was enhanced when cells were treated with LMB (Fig. 3A) and also in CRM1-suppressed cells (Fig. 3B). The interaction between endogenous Smurf2 and CRM1 was confirmed by immunoprecipitation (Supplementary Fig. S3A), and the binding of the two proteins was blocked by the treatment of LMB (Fig. 3C). We introduced alanine mutations at I632 and V634, which are located in the putative nuclear export sequence of Smurf2, which is recognized by CRM1 (20, 21), and checked how these mutations would affect the Smurf2 localization. The mutant did not bind to CRM1 as determined by immunoprecipitation (Fig. 3D). The mutant also showed increased retention in nucleus compared with the wild type (Supplementary Fig. S3B), further validating the significance of these residues for the CRM1-dependnet nuclear export of Smurf2.

Next, we checked whether AIMP2 would affect the binding of CRM1 to Smurf2 using *in vitro* pulldown assay and confirmed that AIMP2 inhibits the interaction between Smurf2 HECT domain and CRM1 in a dose-dependent manner (Fig. 3E). To see whether binding of AIMP2 to Smurf2 is essential for this effect, we compared the effect of AIMP2 WT and Smurf2-binding defective PM2 mutant on the Smurf2–CRM1 interaction by coimmunoprecipitation. In contrast to AIMP2 WT, the mutant did not suppress the binding of Smurf2 to CRM1 (Fig. 3F). We also examined how AIMP2 would affect the nuclear levels of Smurf2 by cell fractionation. The nuclear level of Smurf2 was reduced in AIMP2$^{-/-}$ (KO) MEFs (Fig. 3G) and AIMP2-suppressed cells (Supplementary Fig. S3C). Although the ectopic expression of AIMP2 WT increased the nuclear level of Smurf2, the effect was not shown in Smurf2-binding defective AIMP2 PM2 mutant (Supplementary Fig. S3D). All of these results suggest that AIMP2 would suppress nuclear export of Smurf2 by inhibiting the interaction of Smurf2 with CRM1.

Smurf2–AIMP2 complex increases TβRI level

Smurf2 exported from nucleus induces the ubiquitination of TβRI, deteriorating TGFβ signal (10). As AIMP2 holds Smurf2 in nucleus, the complex formation of the two proteins could enhance the stability of TβRI. To see this possibility, we compared TβRI levels between AIMP2-overexpressed and -suppressed cells or between AIMP2$^{+/+}$ (WT) and AIMP2$^{-/-}$ (KO) MEF cells and found that the TβRI levels showed the positive relationship to the level of AIMP2 (Fig. 4A). However, mRNA expression of TβRI was not much changed by AIMP2 (Fig. 4B), indicating that the effect of AIMP2 on TβRI level occurs at protein level. The AIMP2-dependent regulation of TβRI stability was further examined by pulse-chase experiments. The results showed that the TβRI stability was positively correlated with the expression levels of AIMP2 (Fig. 4C and D). When we repeated the same experiments with AIMP2 MEFs, the reduced stability of TβRI was also observed in AIMP2 KO cells (Fig. 4E).

We tested whether AIMP2 would affect the ubiquitination of TβRI and found that AIMP2 reduced the ubiquitination of TβRI (Fig. 4F). Conversely, the opposite result was observed when AIMP2 was suppressed with its specific siRNA (Fig. 4G). The significance of AIMP2 on the stability of TβRI was also monitored by the phosphorylation of Smad2, which is the substrate of TβRI. TGFβ-dependent phosphorylation of Smad2 was significantly increased by exogenous supplementation of AIMP2 (Fig. 4H) and reduced by the suppression of endogenous AIMP2 (Fig. 4I). The reduction of Smad2 phosphorylation was also observed in AIMP2 KO MEFs (Supplementary Fig. S4A, left), and it was rescued by exogenous introduction of AIMP2 into AIMP2 KO MEFs (Supplementary Fig. S4A, right). We also tested whether AIMP2 would affect the activation of TGFβ target gene, SBE, using the SBE-dependent luciferase assay and found that AIMP2 wild type and PM3 mutant, but not Smurf2 binding-defective PM1 and PM2 mutants, enhanced the luciferase activity (Fig. 4J). We further confirmed the results above using another luciferase reporter assay in which the reporter expression was dependent on the TGFβ-responsive promoter, 3TP. The luciferase activity showed positive relationship to the expression levels of AIMP2 in AIMP2-overexpressed and -suppressed HeLa cells (Supplementary Fig. S4B) and AIMP2 WT or KO MEF cells (Supplementary Fig. S4C). All of these data strongly suggest that AIMP2 would enhance the TGFβ signal by extending the nuclear localization of Smurf2 and stabilization of TβRI.

TGFβ-induced phosphorylation of AIMP2 for nuclear localization

We next investigated how AIMP2 can be translocated to nucleus upon TGFβ signal. As DNA damage–induced nuclear translocation of AIMP2 involves phosphorylation (15), we tested whether AIMP2 is also phosphorylated upon TGFβ signal. Phosphorylation of AIMP2 was detected on serine residue upon TGFβ1 treatment (Supplementary Fig. S5A). To see whether TGFβ-dependent phosphorylation also takes place in endogenous AIMP2,

(*Continued.*) Strep-AIMP2 was immunoprecipitated (IP) with Strep-tag column from the TGFβ1-treated and -untreated cells, and coprecipitated E3 ligases were determined by immunoblotting with the antibodies against their tags. The activity of TGFβ1 treatment was confirmed by phosphorylation of Smad2 in the whole cell lysates (WCL). Mock, immunoprecipitation with nonspecific IgG. C, the TGFβ-treated and -untreated HeLa cells were separated to cytosol (Cyto) and nuclear (Nuc) fractions, and the interaction of endogenous AIMP2 and Smurf2 was tested by coimmunoprecipitation using anti-Smurf2 antibody. HSP90 and YY1 were used as the markers for cytosolic and nuclear fractions, respectively. The activity of TGFβ signal was validated by the phosphorylation of Smad2. D, GST-Smurf2 and GST alone were mixed with *in vitro*–translated AIMP2 that was labeled with [^{35}S]methionine. Smurf2 was pulled down with glutathione-sepharose beads, and coprecipitated AIMP2 was detected by autoradiography. Arrows, GST proteins. E, HeLa cells expressing GFP or GFP-AIMP2 and RFP-Smurf2 were treated with TGFβ1 and their cellular locations were determined by fluorescence confocal microscopy. The nucleus was stained by using DAPI. Each representative image from at least five cell images are shown here. F, schematic diagram showing the arrangement of functional domains in AIMP2 (GST homology domain) and Smurf2 (C2, WW, and HECT domain). Dashed line, peptide regions involved in the interaction of the two proteins.

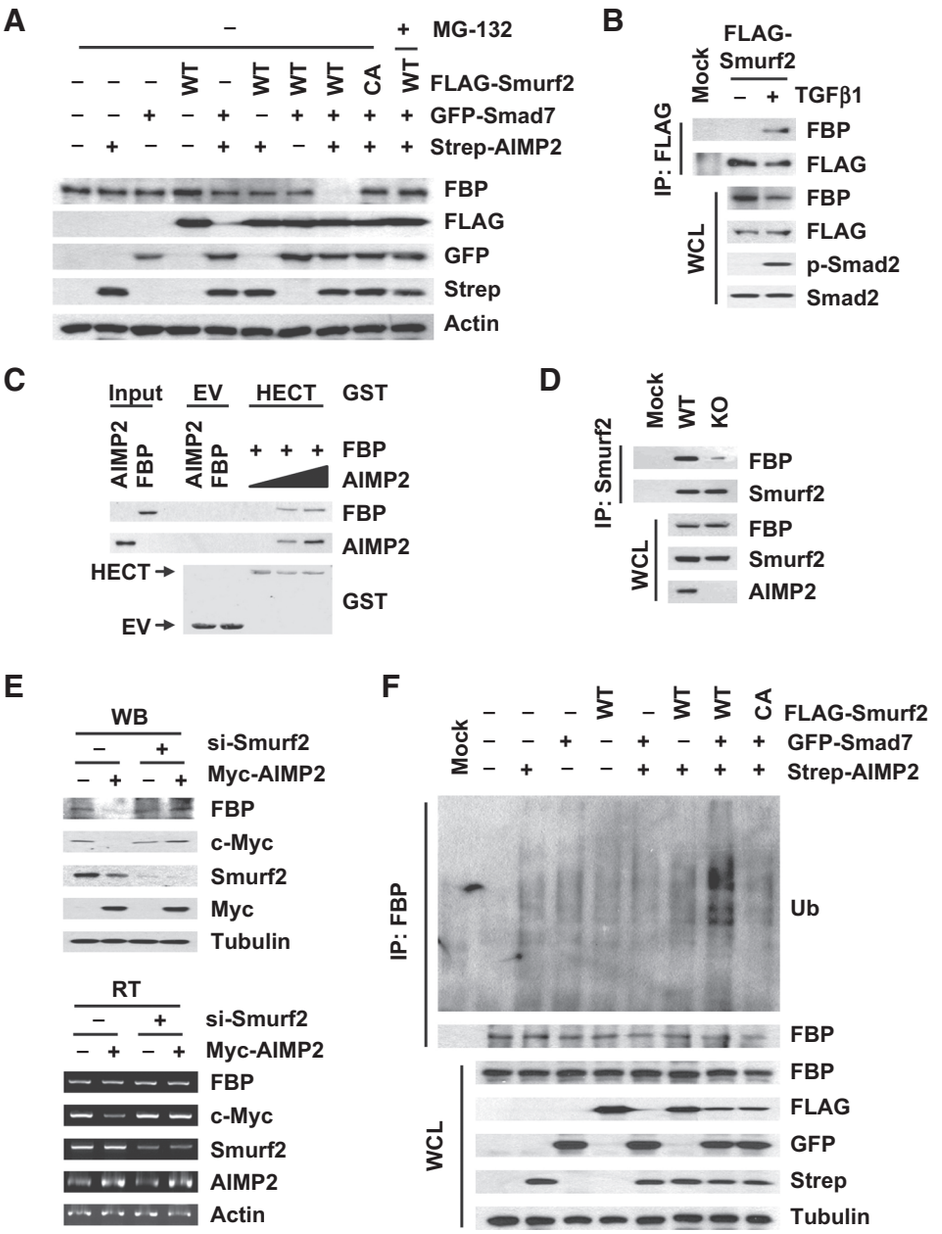

Figure 2.
The requirement of Smurf2 for AIMP2-dependent ubiquitination of FBP. A, different combinations of FLAG-Smurf2, GFP-Smad7, and Strep-AIMP2 were introduced into HeLa cells, and the cells were treated with TGFβ1. Cellular levels of each protein were determined by Western blotting with the indicated antibodies. Smurf2 CA, catalytically inactive mutant of Smurf2. Actin was used as a loading control. B, The TGFβ1-dependent interaction of FLAG-Smurf2 and endogenous FBP was tested in HeLa cells by coimmunoprecipitation (IP). C, GST-fused Smurf2 HECT domain protein was incubated with FBP and the cell extracts containing different levels of AIMP2. GST-fused proteins were precipitated with glutathione-sepharose beads, and coprecipitates with GST proteins were determined by Western blotting with their specific antibodies. D, AIMP2$^{+/+}$ (WT) and AIMP2$^{-/-}$ (KO) MEF cells were treated with MG-132 and TGFβ1. Endogenous Smurf2 was precipitated with its specific antibody, and coprecipitation of FBP was determined by Western blotting with anti-FBP antibody. E, the significance of Smurf2 on the AIMP2-dependent downregulation of FBP was determined by Western blotting (WB) of the related factors (top). The specific siRNA against Smurf2 and Myc-AIMP2 were introduced into HeLa cells. The effect of Smurf2 suppression and AIMP2 overexpression on FBP and c-Myc expression was also determined by RT-PCR (RT, bottom). F, the effect of Smurf2, Smad7, and AIMP2 on ubiquitination of FBP was determined in HeLa cells in which different combinations of the indicated proteins were expressed. The endogenous FBP was precipitated with anti-FBP antibody, and ubiquitination was determined by Western blotting with anti-ubiquitin antibody. EV, empty vector; WCL, whole-cell lysates.

AIMP2 was immunoprecipitated with its specific antibody from TGFβ-treated and control HeLa cells, and phosphorylation at serine residue was determined by Western blotting. The TGFβ-dependent phosphorylation of AIMP2 was observed at serine residue (Supplementary Fig. S5B). As TGFβ signal is known to activate p38MAPK and JNK (22), we tested whether TGFβ-induced phosphorylation of AIMP2 is inhibited by the inhibitors of these kinases. SB202190, an inhibitor of p38MAPK, blocked the phosphorylation of AIMP2, whereas SP600125, an inhibitor of JNK, did not (Supplementary Fig. S5C and S5D, respectively). To determine whether p38MAPK actually phosphorylates AIMP2, we performed *in vitro* kinase assay using TGFβ-activated p38MAPK and observed that p38MAPK directly phosphorylates AIMP2 (Supplementary Fig. S5E). Coimmunoprecipitation of endogenous AIMP2 and p38MAPK and *in vitro* pulldown assay of the two proteins confirmed the direct binding of the two proteins, respectively (Supplementary Fig. S5F and S5G, respectively). The interaction between AIMP2 and p38MAPK was induced by the treatment of TGFβ1 and inhibited by the treatment of SB202190 (Supplementary Fig. S5H). Sequence analysis of AIMP2 using NetPhos 2.0 (23) suggested serine 156, 157, and 160 as putative phosphorylation sites. We thus introduced alanine substitution to these sites to check whether any of these substitutions would affect TGFβ-induced phosphorylation of AIMP2. In *in vitro* kinase assay, alanine substitution at S156, but not at the other sites, reduced p38MAPK-induced phosphorylation (Supplementary Fig. S5I), and the importance of S156 site for TGFβ-induced phosphorylation was further confirmed by the

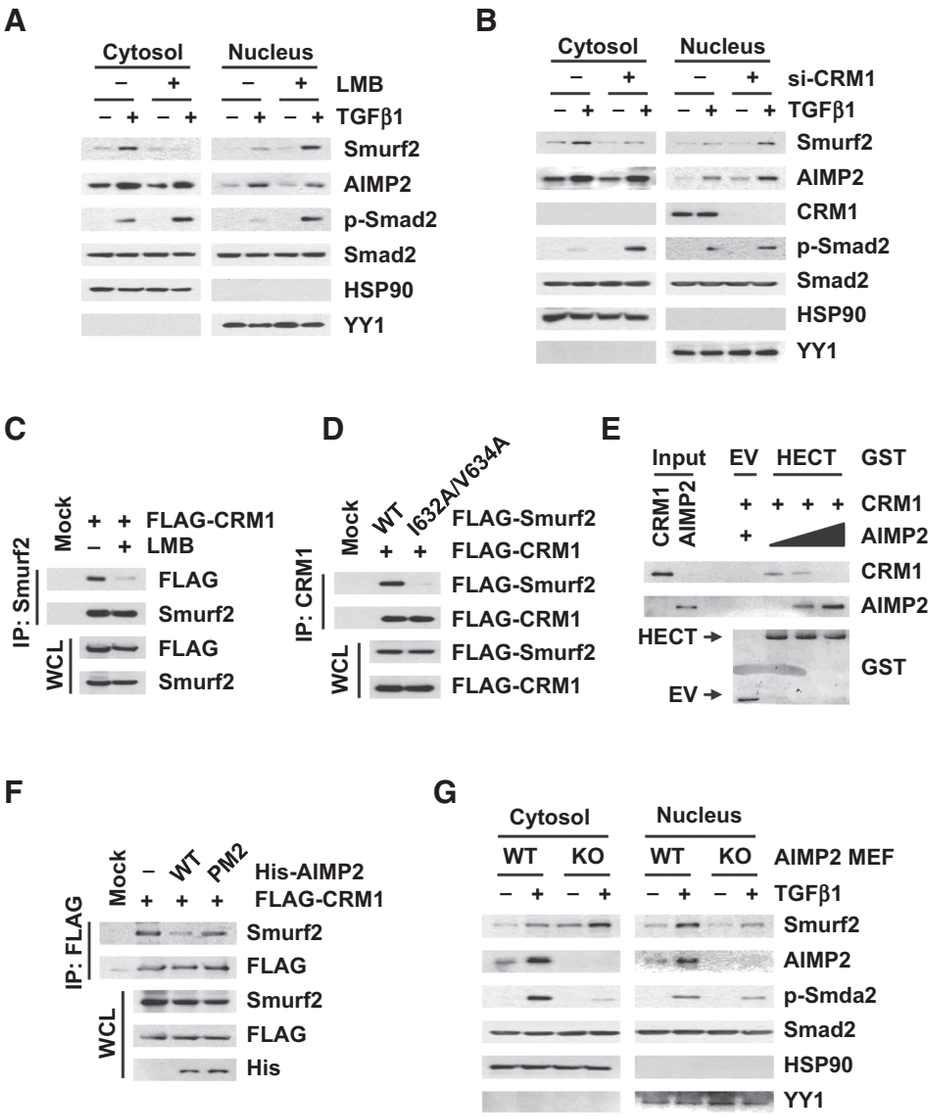

Figure 3.
The role of AIMP2 in nuclear retention of Smurf2. A, HeLa cells treated with different combination of LMB and TGF-β1 were separated to cytosolic and nuclear fractions. The levels of Smurf2 and AIMP2 were determined by Western blotting with their specific antibodies. HSP90 and YY1 were used as the marker for cytosolic and nuclear fractions, respectively. The activity of TGFβ signal was determined by phosphorylation of Smad2. B, HeLa cells treated with si-CRM1 and TGFβ1 were separated to cytosolic and nuclear fractions, and the levels of the indicated factors were determined as above. C, FLAG-CRM1–expressed 293T cells were treated with TGFβ1 in the absence and presence of LMB. Smurf2 was immunoprecipitated (IP) with anti-Smurf2 antibody from cell extracts, and coprecipitation of CRM1 was determined by Western blotting with anti-FLAG antibody. D, FLAG-Smurf2 WT and -I632A/V634A mutant were introduced into FLAG-CRM1–expressed 293T cells. The cells treated with TGFβ1 were subjected to immunoprecipitation with anti-CRM1 antibody, and coprecipitation of Smurf2 was determined by Western blotting with anti-FLAG antibody. E, GST-Smurf2 HECT domain was mixed with the cell extracts, which expressed CRM1 and different levels of AIMP2. Smurf2 was precipitated with glutathione-sepharose beads, and coprecipitation of AIMP2 and CRM1 was determined by Western blotting with their specific antibodies. F, His-AIMP2 WT and point mutant, PM2 (see Supplementary Fig. S1), were introduced into FLAG-CRM1–expressed 293T cells. After treatment with TGFβ1, the cell extracts were subjected to immunoprecipitation with anti-FLAG antibody, and coprecipitation of Smurf2 was determined by Western blotting with anti-Smurf2 antibody. G, $AIMP2^{+/+}$ (WT) and $AIMP2^{-/-}$ (KO) MEFs were treated with TGFβ1 and separated to cytosolic and nuclear fractions, and the levels of Smurf2 and AIMP2 were determined as above. EV, empty vector; WCL, whole-cell lysates.

reduction of TGFβ-dependent phosphorylation in the S156A mutant (Supplementary Fig. S5J). As AIMP2 is normally bound within MSC, we checked whether AIMP2 in MSC could be also phosphorylated by p38MAPK. In *in vitro* kinase assay, we used the purified MSC and the N-terminal 34aa deleted AIMP2 as the reaction substrates and compared their phosphorylation. The results showed that the AIMP2 embedded in MSC could be phosphorylated to the extent similar to the isolated AIMP2 (Supplementary Fig. S5K).

To see the effect of phosphorylation at S156 on the TGFβ signal-dependent nuclear localization of AIMP2, we performed immunofluorescence staining using GFP-AIMP2 WT and the mutants.

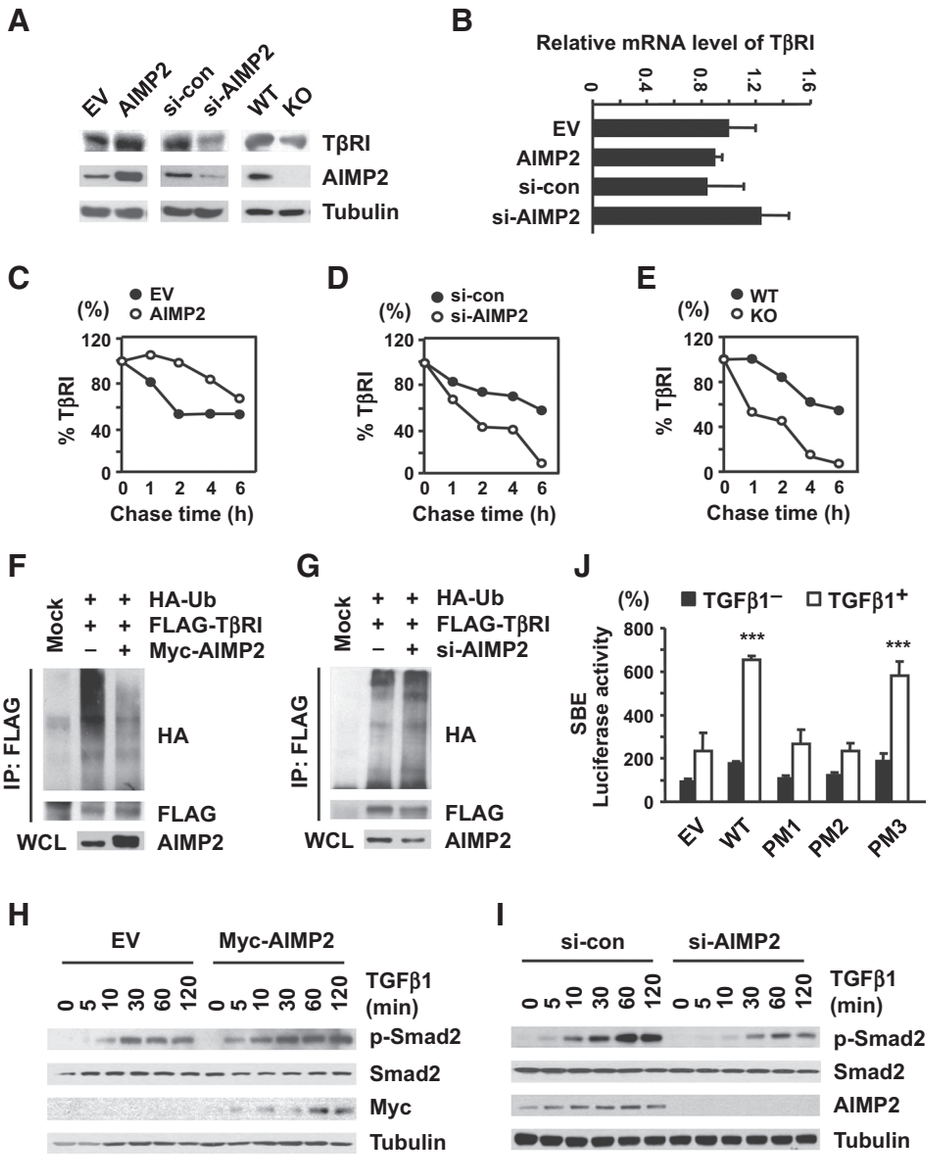

Figure 4.

The effect of AIMP2 on Smurf2-dependent downregulation of TβRI. A, the cellular levels of TβRI were compared by Western blotting in AIMP2-overexpressed and -suppressed HeLa cells and also between AIMP2$^{+/+}$ (WT) and AIMP2$^{-/-}$ (KO) MEFs. B, the mRNA expression of TβRI in HeLa cells as above was monitored by qPCR analysis. C–E, the stability of TβRI in AIMP2-overexpressed (C) and -suppressed (D) HeLa cells and AIMP2 WT and KO MEF cells (E) was monitored by pulse-chase analysis. FLAG-TβRI–introduced cells were incubated in the presence of [^{35}S]methionine. TβRI was immunoprecipitated (IP) with anti-FLAG antibody and subjected to SDS-PAGE. The amounts of TβRI were quantified by densitometry of autoradiographs and are represented by line graphs. F and G, the effect of AIMP2 on the ubiquitination of TβRI was determined in 293T cells that were transfected with FLAG-TβRI and HA-ubiquitin (Ub). AIMP2-overexpressed (F) or -suppressed (G) cells were preincubated with MG132 and treated with TGFβ1. Anti-FLAG antibody was used for immunoprecipitation of TβRI, and the amounts of ubiquitinated TβRI were determined by Western blotting using anti-HA antibody. H and I, time course of TGFβ1-dependent Smad2 phosphorylation and AIMP2 levels was determined by immunoblotting at time interval in AIMP2-overexpressed (H) and -suppressed (I) HeLa cells. J, AIMP2 WT and mutants (PM1-3; see Supplementary Fig. S1A) were introduced into SBE-luciferase–expressing HeLa cells. The cells were untreated or treated with TGFβ1, and the luciferase activities were measured. The experiments were performed three times. Error bars, SD (***, $P < 0.001$). EV, empty vector; WCL, whole-cell lysates.

The TGFβ-dependent nuclear localization of AIMP2 WT was apparent (Supplementary Fig. S6A, top). However, the S156A mutant was not detected in nucleus regardless of TGFβ signal, whereas the S156D mutant, phosphorylation-mimetic form, showed the increased nuclear localization (Supplementary Fig. S6A, middle and bottom, respectively). The similar results were also obtained by Western blotting of the cytosolic and nuclear fractions (Supplementary Fig. S6B). For the incapability of nuclear localization, the S156A mutant could not increase ubiquitination of FBP compared with AIMP2 WT or S156D

mutant (Supplementary Fig. S6C). The results above showed that AIMP2 level could be increased by TGFβ signal (Fig. 4H and I). We thus investigated whether TGFβ-induced phosphorylation at S156 would affect the stability of AIMP2. We first checked whether AIMP2 transcription is affected by TGFβ treatment in HeLa cells by RT-PCR and found no difference in AIMP2 transcript levels after TGFβ treatment (Supplementary Fig. S6D), indicating that TGFβ-induced change of AIMP2 level is not at transcription level. We then transfected AIMP2 WT, S156A (phosphorylation defective) and S156D (phosphorylation mimetic) mutants in 293T cells and treated the cells with cycloheximide to block *de novo* protein synthesis to see whether AIMP2 stability is affected by TGFβ signal. The stability of AIMP2 WT was increased by TGFβ treatment (Supplementary Fig. 6E, top). In contrast, the stability of AIMP2 S156A and S156D mutants was decreased and increased, respectively, compared with the AIMP2 WT, although the stability of both mutants was TGFβ dependent (Supplementary Fig. S6E).

Although exogenous supplementation of AIMP2 WT and S156D mutant increased the interaction of FBP with Smurf2, introduction of AIMP2 S156A mutant gave little effect (Supplementary Fig. S7A). In addition, AIMP2 WT and S156D mutant, but not S156A mutant, inhibited the interaction of Smurf2 with CRM1 (Supplementary Fig. S7B). We checked whether the S156A or D mutation would directly inhibit the interaction of AIMP2 with Smurf2 using *in vitro* synthesized AIMP2 and GST-Smurf2 HECT domain. AIMP2 WT and the two mutants showed little difference in the binding ability to Smurf2, suggesting that the mutations did not affect the binding affinity of AIMP2 to Smurf2 (Supplementary Fig. S7C). As AIMP2 makes interactions with a few components within MSC, including aspartyl-tRNA synthetase (DRS; refs. 13, 24), we tested how the S156 mutations would affect the interaction of AIMP2 with DRS. The S156D mutant showed the reduced binding to DRS, whereas the S156A mutant showed the DRS binding similar to the wild type (Supplementary Fig. S7D). When we monitored the cellular interaction of AIMP2 WT and the two mutants with MSC via DRS as the representative interacting partner, AIMP2 WT showed TGFβ-dependent dissociation from DRS (Supplementary Fig. S7E). However, regardless of TGFβ signal, AIMP2 S156A remained bound to DRS, whereas AIMP2 S156D did not show the binding to DRS. We also examined the effect of S156 mutations on the interaction of AIMP2 with the different components of MSC, such as glutamyl-prolyl-tRNA synthetase (EPRS) and lysyl-tRNA synthetase (KRS) as well as DRS (13, 24), using *in vitro* pulldown assay. Although EPRS and KRS were copurified with all of AIMP2 WT and the two mutants, DRS was copurified only with AIMP2 WT and S156A mutant, but not with AIMP2 S156D mutant (Supplementary Fig. S7F). To see whether the S156D mutation would reduce the association of AIMP2 with MSC, we introduced each of AIMP2 WT and the two mutants into HeLa cells. The MSC was immunoprecipitated using the anti-EPRS antibody, and coprecipitation of AIMP2 was determined by anti-Strep antibody. Although the majority of AIMP2 WT and S156A mutant was detected in the immunoprecipitates of EPRS, AIMP2 S156D mutant was mainly detected in the immunodepleted supernatant (Supplementary Fig. S7G), demonstrating the reduced association of AIMP2 S156D mutant with MSC. The effect of the S156 mutations on the association of AIMP2 with MSC was also compared by gel filtration of MSC. Each of Strep-AIMP2 WT and the two mutants was expressed in the control and TGFβ-treated HeLa cells. The cellular proteins were subjected to gel filtration, and the eluted fractions were separated by SDS-PAGE. Although Strep-AIMP2 WT was mainly coeluted with EPRS and KRS in the control cells, a portion of MSC-bound AIMP2 was decreased, resulting in concomitant increase of AIMP2 in the low molecular weight fractions when the cells were treated with TGFβ1 (Supplementary Fig. S7H, top). These results suggest that the dissociation of AIMP2 from MSC is induced by TGFβ signal, although we do not exclude the possibility that TGFβ-dependent phosphorylation could prevent the association of *de novo* synthesized AIMP2 with MSC. However, regardless of TGBβ signal, AIMP2 S156A mutant was mainly coeluted with the two other components of MSC (Supplementary Fig. S7H, middle), while a large portion of AIMP2 S156D mutant was constitutively detected in low molecular weight fractions (Supplementary Fig. S7H, bottom). All of these results suggest that S156 phosphorylation would reduce the association of AIMP2 with MSC.

Structural analysis of AIMP2 for nuclear translocation and molecular interactions

Knowing the functional significance of S156 phosphorylation, we investigated the structural feature of S156 in the crystal structure of AIMP2. AIMP2, comprised of 320 amino acids, serves as a scaffold protein for the assembly of the MSC. Its N-terminal region (1–45) binding to KRS does not have a regular secondary structure (Fig. 5A; ref. 25). The next part (46–114) contains a heptad repeat region (L52-I80) forming a coiled-coil structure for the interaction to AIMP1 (26). The remaining part of AIMP2 (115–320) forms a GST domain, the structure of which was determined as a complex with the GST domain of EPRS (1–175), which is one of the interacting partners in the MSC (27). In the crystal structure (PDB 5A34), GST domains of AIMP2 and EPRS form a canonical GST dimer (Fig. 5B), and the structure revealed that the peptide region from T90 to K320 of AIMP2 (AIMP2ΔN89) has a flexible N-terminus and a canonical GST domain consisting of GST-N and GST-C subdomains. K120-G222 comprising a 5-stranded β-sheet and the first three α-helices organize a GST-N subdomain, whereas N226-K320 consisting of the remaining five α-helices makes a typical GST-C domain (Fig. 5C and D). The N-terminal T90-L106 was invisible, suggesting a disordered region, while D107-L119 forms a flexible loop (Fig. 5D). AIMP2 has one more strand (β2) and one more helix (α2) between the first helix and following strand in typical GST-N domain, which contains 4-stranded β-sheet (Fig. 5C). The β2 strand-loop-α2 helix motif is only found in AIMP2 and S156 is located at the β2-α2 loop. This loop (^{155}HSSVKSV^{161}) is positioned at an edge of GST-N subdomain and stabilized with hydrogen bonds and hydrophobic interactions within the subdomain (Fig. 5E). The amide group of H155 and the hydroxyl group of S157 are hydrogen bonded to the main chain of W189 and N191, respectively. Two valine side chains in the loop (V158 and V161) participate in a hydrophobic interaction with neighboring residues (W189, L165, L166, and P128). The hydroxyl group of S156 faces to the solvent in the edge of domain and could be accessible for phosphorylation (Fig. 5E).

Metazoan MSCs contain AIMP2 homologs in addition to the enzyme components. Sequences of AIMP2 homologs from various metazoan members (human, mouse, dolphin, sparrow, snake, frog, zebrafish, fly, and sea urchin) were aligned (Supplementary Fig. S8). Although there is a variance in the N-terminal part of AIMP2, the regions for heptad repeat and GST domain are well conserved among those species. In the GST domain,

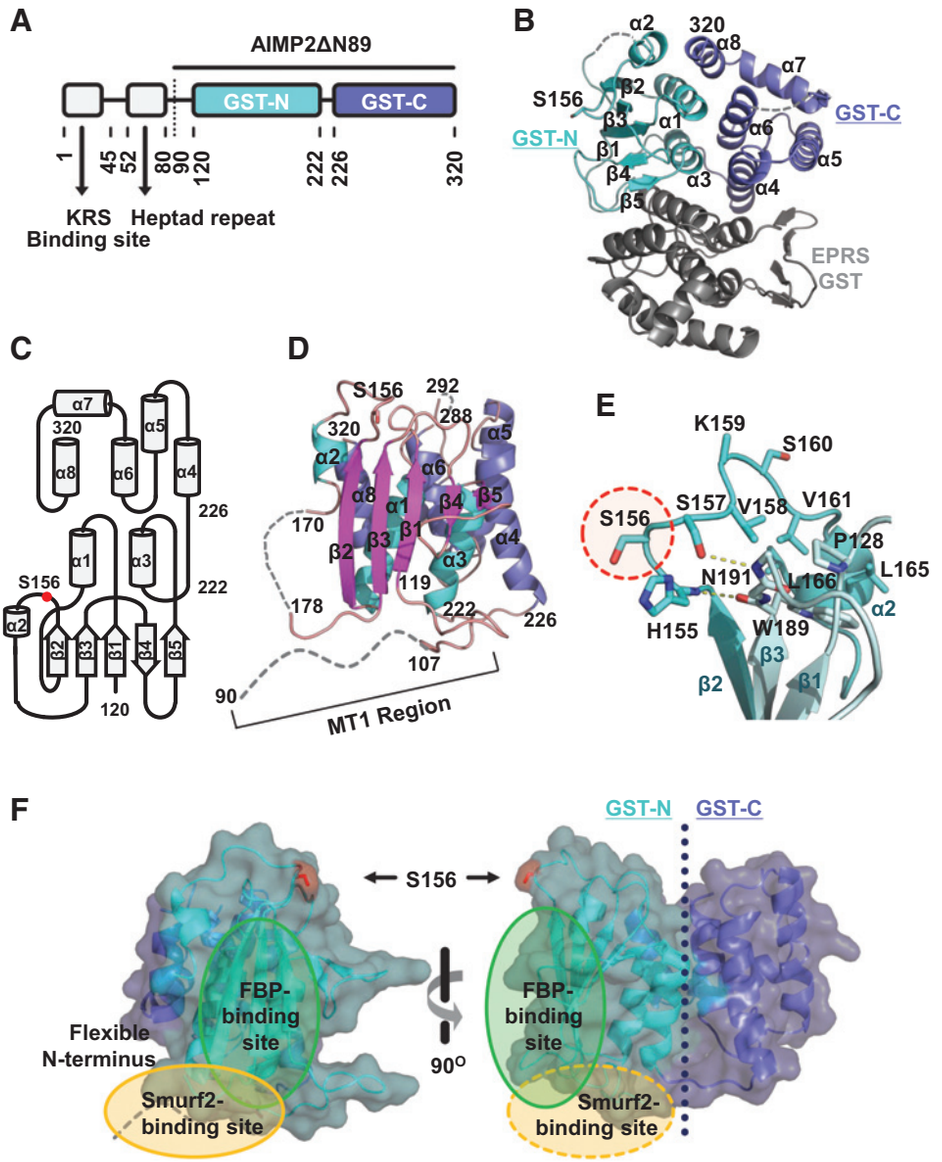

Figure 5.
Structural analysis of AIMP2 and its predicted interactions with Smurf2 and FBP. A, schematic representation of the functional domains in AIMP2. KRS-binding motif and heptad repeat are at its N-terminus, and a GST domain comprised of GST-N and GST-C is at its C-terminus. B, ribbon diagram of AIMP2 GST domain. The GST domain of AIMP2 consists of a 5-stranded β-sheet and eight α-helices. GST-N (cyan) subdomain comprises the five β-sheet and the first three α-helices, whereas GST-C (slate) subdomain contains the last five α-helices. The side chain of S156 is shown as a stick. AIMP2ΔN89 and the GST domain of EPRS (gray) form a canonical GST dimer. C, topology diagram of AIMP2 GST domain. The strand order of the β-sheet in the GST-N domain (120–222) is 2-3-1-4-5. A motif comprising β2 strand and α2 helix is inserted between the first α helix and following β strand of the canonical GST domain containing 4-stranded β-sheet. S156 (red dot) is located at the loop connecting β2 strand and α2 helix. D, the structure contains a 5-stranded β-sheet (magenta) and three α-helices (cyan) for the GST-N and five helices (slate) for the GST-C. Three regions (90–106, 171–177, and 289–291) are disordered with invisible electron density (dot lines). The MT1 region contains a disordered region (90–106) and a flexible loop (107–120). E, the loop (^{155}HSSVKSV^{161}) connecting β2 and α2 in the GST-N is stabilized with hydrogen bonds and hydrophobic interactions. The hydroxyl group of S156 in the loop faces to the solvent. F, spatial arrangement of Smurf2 and FBP-binding sites in AIMP2. A peptide region (yellow circle) in the front of the GST-N subdomain and one side of the β-sheet (green circle) in the GST-N subdomain are the binding sites for Smurf2 and FBP, respectively. The hydroxyl group (red) at S156 is shown with sticks.

the conserved residues are mostly for the hydrophobic cores of GST-N and GST-C subdomains, as well as for the interaction of two subdomains. Interestingly, S156 in the β2-α2 connecting loop is well conserved, suggesting its functional significance.

MT1 region (84–119) of AIMP2 is a motif for the binding to the Smurf2 HECT domain, and the mutational analysis indicated that the residues in the N-terminal part of this region are important for the interaction (see Supplementary Fig. S1).

According to the crystal structure, this N-terminal part of MT1 is disordered, whereas its C-terminal part forms a flexible loop near to the GST domain (Fig. 5D). Negatively charged residues are rich in the N-terminal part of MT1 (P83-P98), and hydrophobic residues are between the negatively charged residues (Supplementary Fig. S8). In the crystal structure of HECT domain of Smurf2, the large subdomain of N-lobe has a groove that has a hydrophobic pocket surrounding by positive potential regions (Supplementary Fig. S9A; ref. 10). This pocket would be suitable to bind the N-terminal part of MT1 in AIMP2 (Supplementary Fig. S9B), although experimental validation is needed. MT2 region (120–155), comprising β1 to β2 strand, is shown to bind to FBP (see Supplementary Fig. S2 and Fig. 5C), implying that the β-sheet could be the binding interface. Thus, the GST-N subdomain of AIMP2 appears to play a significant role for the binding to both of Smurf2 and FBP (Fig. 5F). On the basis of the structure, the phosphorylation at S156 is not expected to affect the interactions of AIMP2 and Smurf2 (Fig. 5F), consistently with the results on the AIMP2 interaction with Smurf2 (Supplementary Fig. S7C).

AIMP2 serves as a scaffold protein interacting with multiple components of MSC (13, 24), and its presence is important for the stability and assembly of the whole complex (28). Recently, crystal structures of KRS binding the N-terminus of AIMP2 (25) and AIMP1 forming a complex with RRS (arginyl-tRNA synthetase) and QRS (glutaminyl-tRNA synthetase) were revealed (29). As AIMP1 is anchored to AIMP2 via coiled-coil interaction of leucine zipper (26), RRS and QRS may be located proximal to AIMP2. MRS and AIMP3 are also linked to AIMP2 via EPRS through the tetrameric complex of their GST domains (27). Another critical region in AIMP2 is 193-203 for DRS binding (13), and it is around β4 strand in GST-N, being located near S156. S156D mutant of AIMP2 showed reduced binding to DRS (Supplementary Fig. S7D), suggesting a role of phosphorylation at S156 either in releasing AIMP2 from MSC or in reducing the association of nascent AIMP2 with MSC (Supplementary Fig. S10).

Significance of AIMP2 in TGFβ-dependent cell phenotypes

The results suggest that the interaction of AIMP2 with Smurf2 could augment TGFβ signal via not only c-Myc downregulation but also stabilization of TβRI. We thus assessed the functional significance of AIMP2 in TGFβ-dependent cell phenotypes. First, we checked the effect of AIMP2 on TGFβ-dependent cell-cycle arrest by thymidine incorporation. The TGFβ-dependent growth arrest was augmented by the introduction of AIMP2 (Fig. 6A) and compromised by the suppression of AIMP2 (that would suppress both of MSC-bound and free AIMP2; Fig. 6B). The growth-suppressive activity of TGFβ was also weakened in AIMP2 KO MEFs and restored when AIMP2 was reintroduced (Fig. 6C). The effect of TGFβ was also monitored by the increase of G_1 phase using flow cytometry. The increase of TGFβ-dependent G_1 phase was not observed in AIMP2-suppressed and AIMP2$^{-/-}$ (KO) MEF cells (Fig. 6D and E, respectively).

To further validate the functional significance of AIMP2 for the control of relevant factors in TGFβ signal pathway, we measured the cellular levels of AIMP2 with FBP, c-Myc, TβRI, and p21 in various lung cancer cell lines and observed the overall reverse correlation of AIMP2 with FBP and c-Myc but positive correlation with TβRI and p21 (Fig. 6F). We introduced AIMP2 WT, S156A and S156D mutants into A549 and HCC44, which show relatively low AIMP2 levels. Overexpression of AIMP2 WT and S156D mutant reduced FBP and increased TβRI and p21, but S156A mutant did not (Fig. 6G, top). We also checked the transcriptional level of the upper molecules in the same cells. Transcription of c-Myc, the target gene of FBP, and p21, the target gene of TGFβ signal, is reduced and augmented, respectively, by the overexpression of AIMP2 (Fig. 6G, bottom).

Significance of AIMP2 in tumor-suppressive TGFβ signaling

To elucidate the functional significance of AIMP2 for tumor-suppressive activity of TGFβ signal, we generated A549 stable cell line expressing AIMP2 WT, S156A, and S156D mutants and compared their effect on cell proliferation using real-time monitoring system. The S156A mutant–expressing cells showed the highest cell growth, whereas the S156D mutant suppressed cell growth compared with other cells (Fig. 7A). We then compared whether these mutants would affect cell transformation by monitoring anchorage-independent colony formation. The S156A mutant–expressing cells generated the highest number of the colonies (Fig. 7B). We also evaluated the effect of S156A mutation on tumor formation *in vivo*. A549 cells expressing each of AIMP2 WT, S156A, S156D, and empty vector were subcutaneously injected into the back of nude mice and analyzed tumor formation. Although the empty vector–transfected cells produced tumors in five of ten mice, the AIMP2 WT-expressing cells generated tumors only in two mice (Fig. 7C–E). The S156A mutant–expressing cells generated tumors in seven of ten mice, whereas the S156D mutant gave no tumor (Fig. 7C–E). The average tumor weights were highest in the cells expressing S156A mutant (Fig. 7F), while body weights of each group showed little variation (Fig. 7G). The cellular levels of FBP, c-Myc, TβRI, and AIMP2 were determined in the isolated tumors. At the similar levels of AIMP2, the WT-expressing cells showed the low levels of c-Myc and FBP, but high level of TβRI, whereas the S156A mutant gave the opposite results (Fig. 7H). All of these results suggest that the TGFβ-dependent phosphorylation of AIMP2 is critical to mediate growth-suppressive activity of TGFβ signal and its disturbance, as in the case of the S156A-mutant, whose overexpression could promote tumor formation.

Discussion

TGFβ signal is known to suppress tumor formation (30, 31), and disturbance of its negative feedback via the Smurf2–Smad7 complex is reported in many cancers (9, 32). Here, we showed that the role of Smurf2 in TGFβ signal can be reversed by AIMP2 to forward direction. Namely, Smurf2 is guided to FBP by AIMP2, leading to the downregulation of c-Myc (Fig. 2). At the same time, its nuclear export is inhibited by AIMP2 that blocks the interaction of Smurf2 with CRM1, thereby stabilizing TβRI that enhances Smad2 phosphorylation and the target gene expression (Fig. 4H–J). For these mechanisms, the increase of AIMP2 would induce Smad target genes as well as suppress c-Myc target genes (Supplementary Fig. S11).

AIMP2 was previously shown to mediate a couple of different signaling pathways that have implications in the control of cancer. For instance, AIMP2 protects p53 from MDM2-mediated degradation and promotes cell death in response to DNA damage (15). AIMP2 also drives TNFα signal to apoptotic direction via downregulation of TRAF2 (16). Here, we show that AIMP2 enhances growth-arresting TGFβ signal by directional guidance of Smurf2 in nucleus. Despite these multifaceted activities of AIMP2, clinical

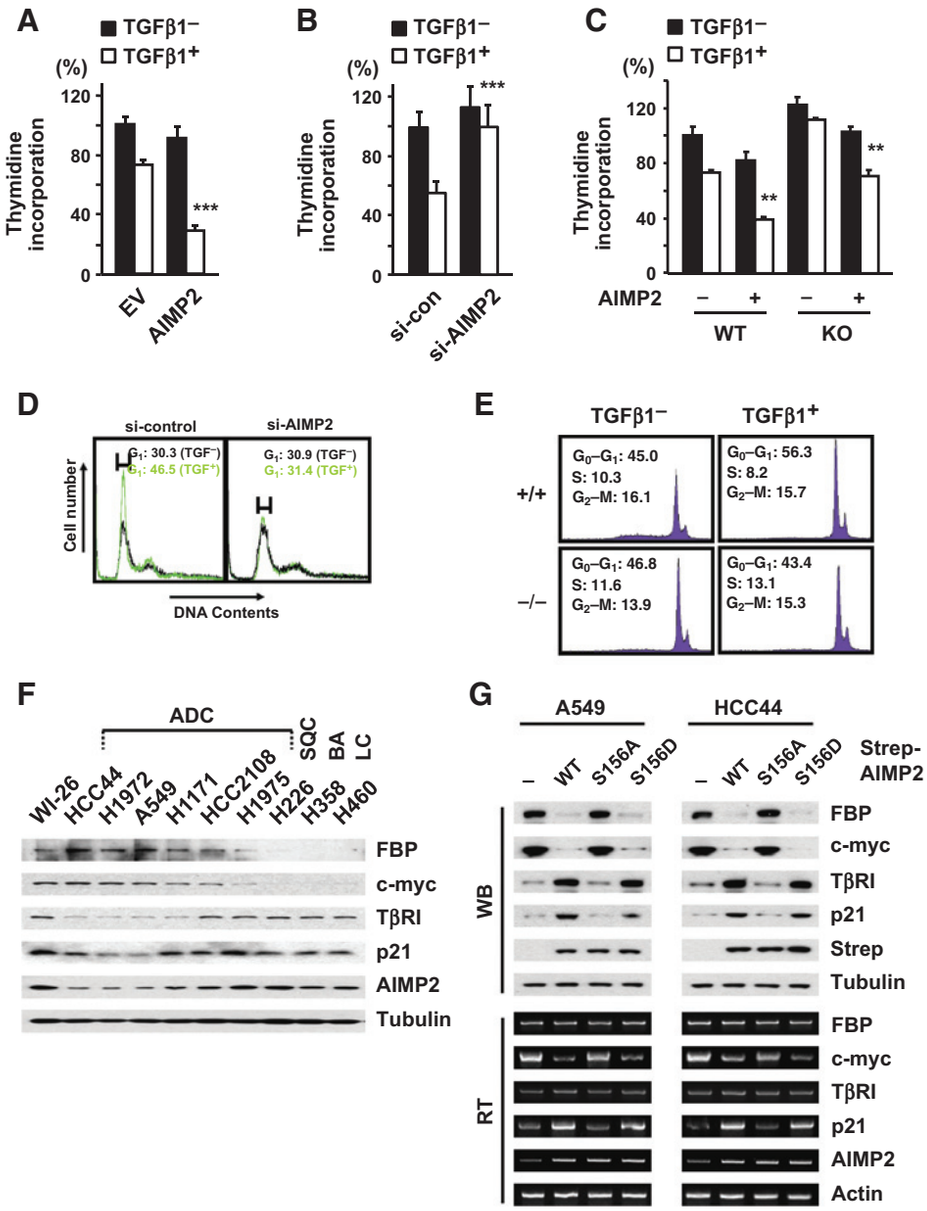

Figure 6.
Significance of AIMP2 for TGFβ1-induced cell phenotypes. A–C, the effects of AIMP2 overexpression (A) and suppression (B) on A549 cell proliferation were determined by thymidine incorporation in the presence and absence of TGFβ1. The effect of AIMP2 on TGFβ1-dependent growth arrest was also determined as above between AIMP2$^{+/+}$ (WT) and AIMP2$^{-/-}$ (KO) MEF cells (C). All the experiments (A–C) were repeated three times. Error bars, SD (in A and B, ***, $P < 0.001$; in C, **, $P < 0.01$). D, TGFβ signal-mediated cell cycle was monitored by FACS analysis in HeLa cells that were transfected with control and anti-AIMP2 siRNAs. E, AIMP2$^{+/+}$ (WT) and AIMP2$^{-/-}$ (KO) MEFs were treated with TGFβ1, and the cell cycle was monitored as above. F, the cellular levels of FBP, c-Myc, TβRI, p21, and AIMP2 were determined in different non–small cell lung cancer cell lines by Western blotting (WB) with their specific antibodies. ADC, adenocarcinoma; SQC, squamous carcinoma; BA, bronchioloalveolar carcinoma; and LC, large cell carcinoma. RT, RT-PCR. Tubulin was used as a loading control. G, the effect of Myc-AIMP2 WT, S156A, and D mutants on the protein (top) and transcription (bottom) levels of FBP, c-Myc, TβRI, and p21 was tested in A549 and HCC44 cells.

relevance of AIMP2 to cancer has not been investigated much. In this regard, it is worth noting that cancer-associated expression of AIMP2-DX2, an alternative splicing variant of AIMP2, and its tumorigenic activity have been demonstrated in various cancers (33–35). As this variant compromises the tumor-suppressive activities of AIMP2 in the p53 and TNFα pathways, it would be interesting to see whether this variant would also affect the tumor-suppressive interaction of AIMP2 with Smurf2 in nucleus. Also, S156F mutation was reported in prostate cancer patients, although the mutation frequency is not high (36, 37), and here, we discovered the reduced expression of AIMP2 in some of the lung cancer cell lines, especially in some of adenocarcinoma cells, with enhanced c-Myc and reduced TβRI levels (Fig. 6F), further supporting the significance of AIMP2 in TGFβ signaling. This work also shows a tumor-promoting mutation at S156 of AIMP2 that disturbs its nuclear function (Fig. 7), implying a potential existence of oncogenic mutations at the structural gene of AIMP2.

Although AIMP2 is normally bound to MSC, the nuclear localization of AIMP2 would be achieved either by its dissociation from MSC or by *de novo* synthesis of AIMP2, which is directly guided to nucleus without binding to MSC. In this work, we showed that AIMP2 is phosphorylated at S156 site by TGFβ-activated p38MAPK for its nuclear function via Smurf2. The phenotypic effect of the phosphorylation-defective mutant on cell growth, transformation, and tumor promotion *in vivo* suggests the functional significance of the nuclear interaction of AIMP2 with Smurf2 in the tumor-suppressive TGFβ

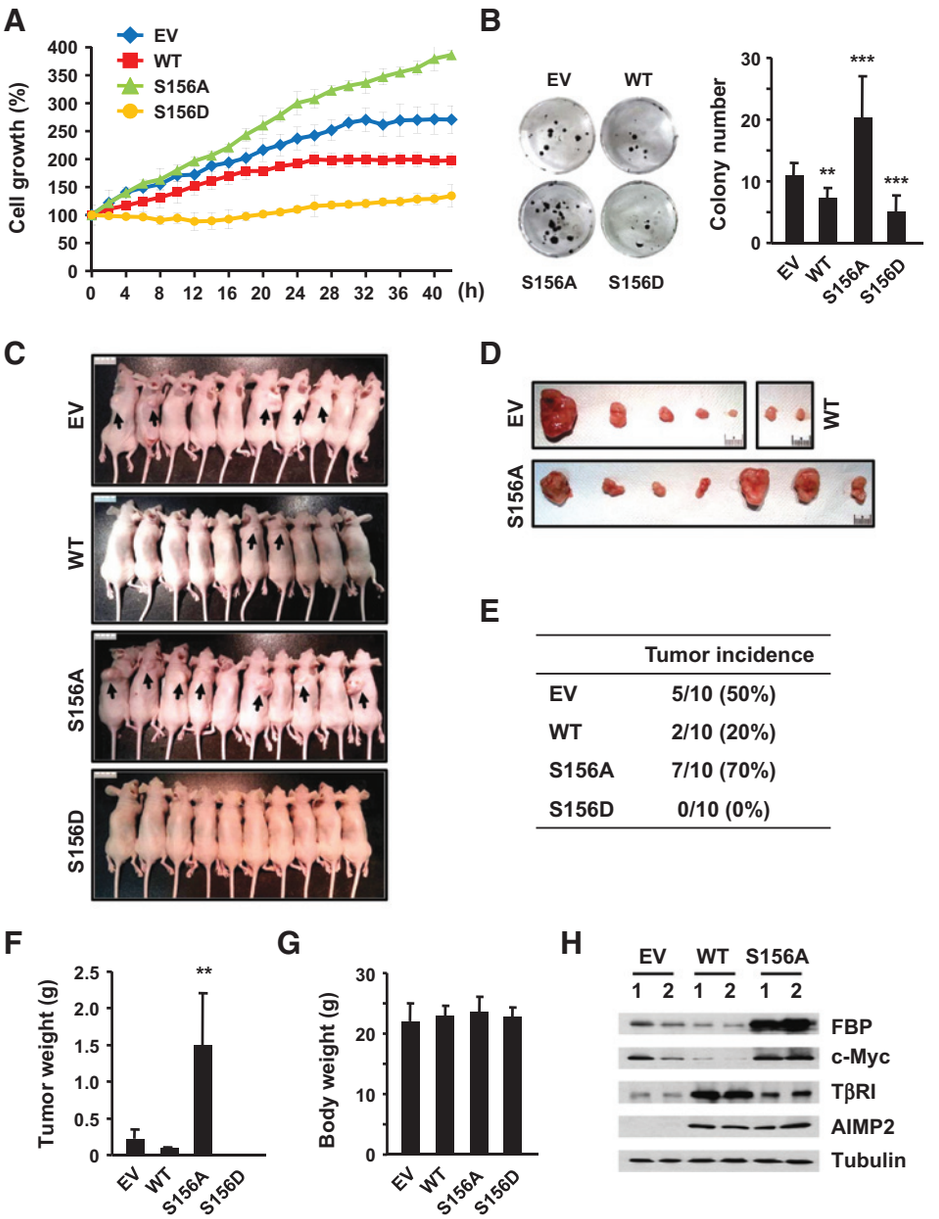

Figure 7.
Effect of AIMP2 S156A mutation on cell and tumor growth. A, A549 cells stably expressing AIMP2 WT, S156A, and D mutants were compared for their cell growth by real-time cell monitoring system for 42 hours. The experiments were performed three times. Error bars, SD. B, same cells as above were tested for anchorage-independent colony-forming ability. The same number of each cell line was embedded into the medium, and the resulting colonies were displayed as bar graphs with error bars of SD (right, **, $P < 0.01$; ***$P < 0.001$) from three independent experiments. Left, representative photos are shown. C–H, the cells above were compared for their ability to induce tumors in nude mice. The cells above were subcutaneously inoculated on the back of nude mice. After two months from injection, mice were sacrificed and the tumors analyzed. The photos of the mouse-embedded and isolated tumors are presented in C and D, respectively. Tumor incidence of each group was summarized as a table in E. Tumor and body weights are presented as bar graphs with error bars of SD in F and G, respectively (in F, **, $P < 0.01$). H, the cellular levels of FBP, c-Myc, TβRI, and Myc-AIMP2 were determined by Western blotting with the indicated antibodies. EV, empty vector.

signaling. Interestingly, the phosphorylation-defective mutant gave dominant effect on tumor promotion despite the fact that the cells would still retain the AIMP2 WT allele. Perhaps, the mutant would compete out AIMP2 WT from MSC, resulting in the reduction of functional AIMP2. Considering the haploinsufficiency of AIMP2 function (17), coexpression of AIMP2 WT and S156A mutant would mimic the situation of AIMP2 haploid, which showed increased tumor susceptibility. This finding suggests a possibility that mutations of AIMP2 disrupting its TGFβ signal-mediating activities could promote tumorigenesis. Interestingly, the AIMP2 mutants, such as G209S or E97D, P98L, and T99S, that could not bind Smurf2 (Supplementary Fig. S1E), were also found in cancer cell lines (15). It would be interesting to see whether these mutants would also induce the phenotypes as shown in this work.

Disclosure of Potential Conflicts of Interest

S.-J. Kim is the Chief Technology Officer at TheragenEtex Co. No potential conflicts of interest were disclosed by the other authors.

Authors' Contributions

Conception and design: D.G. Kim, M. Guo, J.M. Han, S.-J. Kim, S. Kim
Development of methodology: S.-J. Kim
Acquisition of data (provided animals, acquired and managed patients, provided facilities, etc.): D.G. Kim, J.Y. Lee, H.Y. Cho, B.S. Kang, S.-Y. Jang
Analysis and interpretation of data (e.g., statistical analysis, biostatistics, computational analysis): D.G. Kim, J.Y. Lee, J.-H. Lee, H.Y. Cho, B.S. Kang, M.H. Kim, M. Guo, J.M. Han

Writing, review, and/or revision of the manuscript: D.G. Kim, M. Guo, J.M. Han, S. Kim
Administrative, technical, or material support (i.e., reporting or organizing data, constructing databases): D.G. Kim, J.Y. Lee
Study supervision: J.M. Han, S. Kim

Grant Support

This work was supported by the Global Frontier Project grant (NRF-M3A6A4-2010-0029785 and NRF-2013M3A6A4045813) of National Research Foundation funded by the Ministry of Science, ICT & Future Planning (MSIP) of Korea, a grant from Gyeonggi Research Development Program.

The costs of publication of this article were defrayed in part by the payment of page charges. This article must therefore be hereby marked *advertisement* in accordance with 18 U.S.C. Section 1734 solely to indicate this fact.

Received December 10, 2015; revised February 11, 2016; accepted February 26, 2016; published OnlineFirst April 6, 2016.

References

1. Siegel PM, Massague J. Cytostatic and apoptotic actions of TGF-beta in homeostasis and cancer. Nat Rev Cancer 2003;3:807–21.
2. Massague J.How cells read TGF-beta signals. Nat Rev Mol Cell Biol 2000; 1:169–78.
3. Massague J. TGFbeta in cancer. Cell 2008;134:215–30.
4. Ikushima H, Miyazono K. TGFbeta signalling: a complex web in cancer progression. Nat Rev Cancer 2010;10:415–24.
5. Meulmeester E, Ten Dijke P. The dynamic roles of TGF-beta in cancer. J Pathol 2011;223:205–18.
6. Massague J, Chen YG. Controlling TGF-beta signaling. Genes Dev 2000; 14:627–44.
7. Hayashi H, Abdollah S, Qiu Y, Cai J, Xu YY, Grinnell BW, et al. The MAD-related protein Smad7 associates with the TGFbeta receptor and functions as an antagonist of TGFbeta signaling. Cell 1997;89: 1165–73.
8. Itoh S, ten Dijke P.Negative regulation of TGF-beta receptor/Smad signal transduction. Curr Opin Cell Biol 2007;19:176–84.
9. Izzi L, Attisano L. Regulation of the TGFbeta signalling pathway by ubiquitin-mediated degradation. Oncogene 2004;23:2071–8.
10. Wiesner S, Ogunjimi AA, Wang HR, Rotin D, Sicheri F, Wrana JL, et al. Autoinhibition of the HECT-type ubiquitin ligase Smurf2 through its C2 domain. Cell 2007;130:651–62.
11. Kavsak P, Rasmussen RK, Causing CG, Bonni S, Zhu H, Thomsen GH, et al. Smad7 binds to Smurf2 to form an E3 ubiquitin ligase that targets the TGF beta receptor for degradation. Mol Cell 2000;6:1365–75.
12. Blank M, Tang Y, Yamashita M, Burkett SS, Cheng SY, Zhang YE. A tumor suppressor function of Smurf2 associated with controlling chromatin landscape and genome stability through RNF20. Nat Med 2012;18:227–34.
13. Quevillon S, Robinson JC, Berthonneau E, Siatecka M, Mirande M. Macromolecular assemblage of aminoacyl-tRNA synthetases: identification of protein-protein interactions and characterization of a core protein. J Mol Biol 1999;285:183–95.
14. Park SG, Ewalt KL, Kim S. Functional expansion of aminoacyl-tRNA synthetases and their interacting factors: new perspectives on housekeepers. Trends Biochem Sci 2005;30:569–74.
15. Han JM, Park BJ, Park SG, Oh YS, Choi SJ, Lee SW, et al. AIMP2/p38, the scaffold for the multi-tRNA synthetase complex, responds to genotoxic stresses via p53. Proc Natl Acad Sci U S A 2008;105:11206–11.
16. Choi JW, Kim DG, Park MC, Um JY, Han JM, Park SG, et al. AIMP2 promotes TNFalpha-dependent apoptosis via ubiquitin-mediated degradation of TRAF2. J Cell Sci 2009;122:2710–15.
17. Choi JW, Um JY, Kundu JK, Surh YJ, Kim S. Multidirectional tumor-suppressive activity of AIMP2/p38 and the enhanced susceptibility of AIMP2 heterozygous mice to carcinogenesis. Carcinogenesis 2009;30:1638–44.
18. Duncan R, Bazar L, Michelotti G, Tomonaga T, Krutzsch H, Avigan M, et al. Sequence-specific, single-strand binding-protein activates the far upstream element of C-Myc and defines a new DNA-binding motif. Gene Dev 1994;8:465–80.
19. Kim MJ, Park BJ, Kang YS, Kim HJ, Park JH, Kang JW, et al. Downregulation of FUSE-binding protein and c-myc by tRNA synthetase cofactor p38 is required for lung cell differentiation. Nat Genet 2003;34:330–6.
20. Tajima Y, Goto K, Yoshida M, Shinomiya K, Sekimoto T, Yoneda Y, et al. Chromosomal region maintenance 1 (CRM1)-dependent nuclear export of Smad ubiquitin regulatory factor 1 (Smurf1) is essential for negative regulation of transforming growth factor-beta signaling by Smad7. J Biol Chem 2003;278:10716–21.
21. Fornerod M, Ohno M, Yoshida M, Mattaj IW. CRM1 is an export receptor for leucine-rich nuclear export signals. Cell 1997;90:1051–60.
22. Zhang YE.Non-Smad pathways in TGF-beta signaling. Cell Res 2009;19: 128–39.
23. Blom N, Gammeltoft S, Brunak S. Sequence and structure-based prediction of eukaryotic protein phosphorylation sites. J Mol Biol 1999;294:1351–62.
24. Robinson JC, Kerjan P, Mirande M. Macromolecular assemblage of aminoacyl-tRNA synthetases: quantitative analysis of protein-protein interactions and mechanism of complex assembly. J Mol Biol 2000;304:983–94.
25. Ofir-Birin Y, Fang P, Bennett SP, Zhang HM, Wang J, Rachmin I, et al. Structural switch of lysyl-tRNA synthetase between translation and transcription. Mol Cell 2013;49:30–42.
26. Ahn HC, Kim S, Lee BJ. Solution structure and p43 binding of the p38 leucine zipper motif: coiled-coil interactions mediate the association between p38 and p43. Febs Letters 2003;542:119–24.
27. Cho HY, Maeng SJ, Cho HJ, Choi YS, Chung JM, Lee S, et al. Assembly of multi-tRNA synthetase complex via heterotetrameric glutathione transferase-homology domains. J Biol Chem 2015;290:29313–28.
28. Kim JY, Kang YS, Lee JW, Kim HJ, Ahn YH, Park H, et al. P38 is essential for the assembly and stability of macromolecular tRNA synthetase complex: Implications for its physiological significance. Proc Natl Acad Sci U S A 2002;99:7912–6.
29. Fu Y, Kim Y, Jin KS, Kim HS, Kim JH, Wang D, et al. Structure of the ArgRS-GlnRS-AIMP1 complex and its implications for mammalian translation. Proc Natl Acad Sci U S A 2014;111:15084–9.
30. Ikushima H, Miyazono K. TGF beta signalling: a complex web in cancer progression. Nat Rev Cancer 2010;10:415–24.
31. Massague J.TGF beta in cancer. Cell 2008;134:215–30.
32. Kleeff J, Ishiwata T, Maruyama H, Friess H, Truong P, Buchler MW, et al. The TGF-beta signaling inhibitor Smad7 enhances tumorigenicity in pancreatic cancer. Oncogene 1999;18:5363–72.
33. Choi JW, Kim DG, Lee AE, Kim HR, Lee JY, Kwon NH, et al. Cancer-associated splicing variant of tumor suppressor AIMP2/p38: pathological implication in tumorigenesis. PLoS Genet 2011;7:e1001351.
34. Choi JW, Lee JW, Kim JK, Jeon HK, Choi JJ, Kim DG, et al. Splicing variant of AIMP2 as an effective target against chemoresistant ovarian cancer. J Mol Cell Biol 2012;4:164–73.
35. Lee HS, Kim DG, Oh YS, Kwon NH, Lee JY, Kim D, et al. Chemical suppression of an oncogenic splicing variant of AIMP2 induces tumour regression. Biochem J 2013;454:411–6.
36. Cerami E, Gao J, Dogrusoz U, Gross BE, Sumer SO, Aksoy BA, et al. The cBio cancer genomics portal: an open platform for exploring multidimensional cancer genomics data. Cancer Discov 2012;2:401–4.
37. Forbes SA, Bindal N, Bamford S, Cole C, Kok CY, Beare D, et al. COSMIC: mining complete cancer genomes in the Catalogue of Somatic Mutations in Cancer. Nucleic Acids Res 2011;39:D945–50.